



# Above-threshold ionization by polarization-crafted pulses

Camilo Granados<sup>1,2,3,a</sup>, Enrique G. Neyra<sup>4</sup>, Lorena Rebón<sup>5,6</sup>, and Marcelo F. Ciappina<sup>1,2,3,b</sup>

<sup>1</sup> Department of Physics, Guangdong Technion - Israel Institute of Technology, 241 Daxue Road, Shantou 515063, China  
<sup>2</sup> Technion - Israel Institute of Technology, Haifa 32000, Israel

<sup>3</sup> Guangdong Provincial Key Laboratory of Materials and Technologies for Energy Conversion, Guangdong Technion - Israel Institute of Technology, 241 Daxue Road, Shantou 515063, China

<sup>4</sup> Instituto Balseiro (Universidad Nacional de Cuyo and Comisión Nacional de Energía Atómica) and CONICET CCT Patagonia Norte, Av. Bustillo 9500, Bariloche (RN) 8400, Argentina

<sup>5</sup> Instituto de Física de La Plata, CONICET - CCT La Plata, Diag. 119 e/ 63 y 64, La Plata 1900, Argentina

<sup>6</sup> Departamento de Física, Facultad de Ciencias Exactas, Universidad Nacional de La Plata, La Plata 1900, Argentina

Received 22 July 2024 / Accepted 21 August 2024

© The Author(s), under exclusive licence to EDP Sciences, SIF and Springer-Verlag GmbH Germany, part of Springer Nature 2024

**Abstract.** Coherent light has revolutionized scientific research, spanning biology, chemistry and physics. To delve into ultrafast phenomena, the development of high-energy, highly tunable light sources is instrumental. Here, the photoelectric effect is a pivotal tool for dissecting electron correlations and system structures. Particularly, above-threshold ionization (ATI), characterized by the simultaneous absorption of several photons leading to a final electron energy well above the ionization threshold, has been widely explored, both theoretically and experimentally. ATI decouples laser field effects from the structural information carried by photoelectrons, particularly when utilizing ultrashort pulses. In this contribution, we study ATI driven by polarization-crafted (PC) pulses, which offer precise scanning over the electron momentum, through an accurate change of the polarization state. PC pulses enable the manipulation of photoelectron momentum distributions, opening up new avenues for understanding and harnessing coherent light. Our work explores how structured light could allow for a proper understanding of emitted photoelectrons momentum distributions in order to distinguish between light structure effects and target structure effects.

## 1 Introduction

Coherent light has guided, for the last decades, countless advances in different areas of sciences, ranging from biology to chemistry and physics [1–5]. It is now customary, in many optics laboratories, to explore the frontiers of natural processes at temporal scales close to the electron motion in atoms, molecules and larger structures [3]. This landscape of research is only possible thanks to the development of ultrashort laser pulses with a duration of the order of attoseconds [6–8]. Advances in this technology toward the creation of tabletop setups of higher-energy attosecond light sources, which would allow us to investigate nature on unexplored energy and timescales, are one of the cornerstones of attosecond science.

One of the typical uses of coherent light is the photoelectric effect. Here, both single and multi-photon absorption are key to understand, for example, electron correlations or structural properties of the systems under investigation. The ionization of atoms by

the simultaneous absorption of several photons arises as one of the fundamental nonlinear effects, together with high-harmonic generation (HHG) [9–11], where a complete new chapter of the light–matter interaction was necessary to fully describe the seminal experimental observations [9, 10, 12, 13]. The simultaneous absorption of several photons leading to a final electron energy well above the ionization threshold, known as above-threshold ionization (ATI), has been investigated during several decades both theoretically and experimentally [12, 14]. Understanding photo-absorption processes allows us to decouple the influence of the strong laser field in photoelectron dynamics from the structural information that photoelectrons could carry, especially when very short pulses are used [15]. In this sense, ATI is a well-established phenomenon to study structural properties of the target systems, either atomic or molecular, since it inherits information on the bound-to-free and re-scattering continuum–continuum electronic transitions. With the advent of carrier-envelope-phase (CEP) stabilization mechanisms, the ATI played a paramount role in demonstrating CEP effects in the observed photoelectron spectra. This was proved experimentally by measuring correlation between photoelectrons emitted in opposite directions [16]. Without the

<sup>a</sup> e-mail: [camilo.granados@gtiit.edu.cn](mailto:camilo.granados@gtiit.edu.cn) (corresponding author)

<sup>b</sup> e-mail: [marcelo.ciappina@gtiit.edu.cn](mailto:marcelo.ciappina@gtiit.edu.cn) (corresponding author)

CEP stabilization, the effect on the photoelectron spectra normally averages out because the random phase of the electromagnetic field that each pulse carries. In another interesting application, the diffraction pattern generated by re-scattered electrons was used to infer changes in the molecular bond lengths of oxygen and nitrogen molecules [17]. This self-imaging of molecules provides a powerful technique by which the changes of the molecular bond lengths can be followed in real time [17, 18]. In addition, with the experimental development of laser light carrying angular momentum [19], it is now possible to decouple the multi-scattering nature of ATI from the inter-pulses interference effects. New pulse synthesis thus open the door to investigate, understand and manipulate coherent light with unexplored degrees of freedom [5, 20].

From the theoretical point of view, energy-resolved photoelectron distributions, as well as two-dimensional (2D) photoelectron momentum spectra (the angular distribution of electrons in both the parallel and perpendicular directions with respect to the laser field polarization), can be calculated by solving the time-dependent Schrödinger equation (TDSE) [21–23] or by semiclassical approaches [24]. The three-dimensional TDSE is able to reproduce, with a high degree of accuracy, the experimental results for atomic targets modeled within the single active electron approximation. However, we should mention two main drawbacks, namely (i) that it is computationally expensive and (ii) that is very difficult to extract information about the underlying physical mechanisms. Contrariwise, the strong field approximation (SFA) offers a clear framework for examining the different contributions giving rise to the final photoelectron distributions. Added to this, the SFA is computationally far less expensive yet giving good qualitative results. Furthermore, the solution of the TDSE for all degrees of freedom involved in the problem is often difficult or even impossible to find. By using the SFA, Suárez et al. [10] were able to characterize the ATI process in terms of direct and re-scattered electrons. This is an step forward to fully decouple the distinct contributions to the ATI process and opens a way to extract structural properties of both atomic and molecular targets. More recently, in Ref. [25] it was demonstrated that, by using amplitude-polarization (AP) attosecond pulses, the emitted electron angular momentum could be controlled. The possibility of tailoring the attosecond pulse polarization has the potential to unlock the investigation of complex physical systems.

In this work, we investigate the ATI phenomenon driven by polarization-crafted (PC) pulses, for which AP pulses are a special case. The use of PC pulses allows us to continuously change the electron emission direction and presents an approach to fine-tune the degree of collimation in the photoelectron emission direction. The complete understanding of the highly focused laser-generated electron beams could be useful for extracting information for both the laser pulse itself and the atomic or molecular target.

The manuscript is organized as follows: In Sect. 2, we first define PC laser fields and show how to use their time delay, relative phase and amplitude ratios for crafting their polarization state. In Sect. 3, we present atomic ATI calculations, obtained from the solution of the three-dimensional (3D) TDSE, using two short laser fields with variable time delay and phase between them. Here we show how the different photoelectron momentum distributions closely follows the PC laser field oscillation direction. In Sect. 4, we present the photoelectron momentum distributions using long PC laser pulses and show how by modifying the laser field amplitudes' ratio one can change the photoelectron momentum distributions. Finally, the conclusions are included in Sect. 5.

## 2 Polarization-crafted (PC) laser pulses

We first revise the concept of PC pulses, and then, we show how they can be used to steer the electron dynamics. For this purpose, we compute the photoelectron spectra of an hydrogen atom, when interacting with a laser field synthesized from two 800-nm ultrashort laser fields with variable relative phase, time delay and peak amplitudes between them. Our study is divided in two regimes, depending on the temporal duration of the laser pulses, i.e., we analyze the use of short and long laser pulses. For calculating the photoelectron ATI spectra, we used the Q-PROP 3D TDSE solver [23].

A PC pulse results from the coherent superposition of two linearly polarized orthogonal electromagnetic fields, i.e.,  $\mathbf{E}(t) = E_x(t)\hat{x} + E_y(t)\hat{y}$ , with no restriction on their phases, time delay and amplitudes. This is in contrast to the AP pulses, for which the difference between the CEP phase of both pulses and amplitude of each component is always the same. Here we used  $\sin^2$ -shaped pulses for the numerical results presented in this and the following sections. Thus, each of the electric field components,  $E_x(t)$  and  $E_y(t)$ , can be written as:

$$E_x(t) = E_{0,x} \sin^2\left(\frac{\omega_0 t}{2n_c}\right) \sin(\omega_0 t + \phi_x), \quad (1a)$$

$$E_y(t) = E_{0,y} \sin^2\left(\frac{\omega_0(t - \delta t)}{2n_c}\right) \sin(\omega_0(t - \delta t) + \phi_y), \quad (1b)$$

where  $E_{0,x} = \frac{E_0}{\sqrt{1+\varepsilon^2}}$  ( $E_{0,y} = \frac{\varepsilon E_0}{\sqrt{1+\varepsilon^2}}$ ) is the laser field peak amplitude in the  $x$  ( $y$ )-direction,  $\omega_0$  the laser field central frequency,  $n_c$  the number of total cycles and  $\delta t$  and  $\phi_x$  ( $\phi_y$ ) are the time delay and carrier-envelope phase (CEP) of the  $x$  ( $y$ ) laser field component, respectively.<sup>1</sup> The time delay between the pulses is defined in

<sup>1</sup> Note that our definition contains the conventional elliptical polarized fields for  $\delta t = 0$  and allow us to define the laser intensity as  $I = E_0^2$ , independent of the value of  $\varepsilon$ .

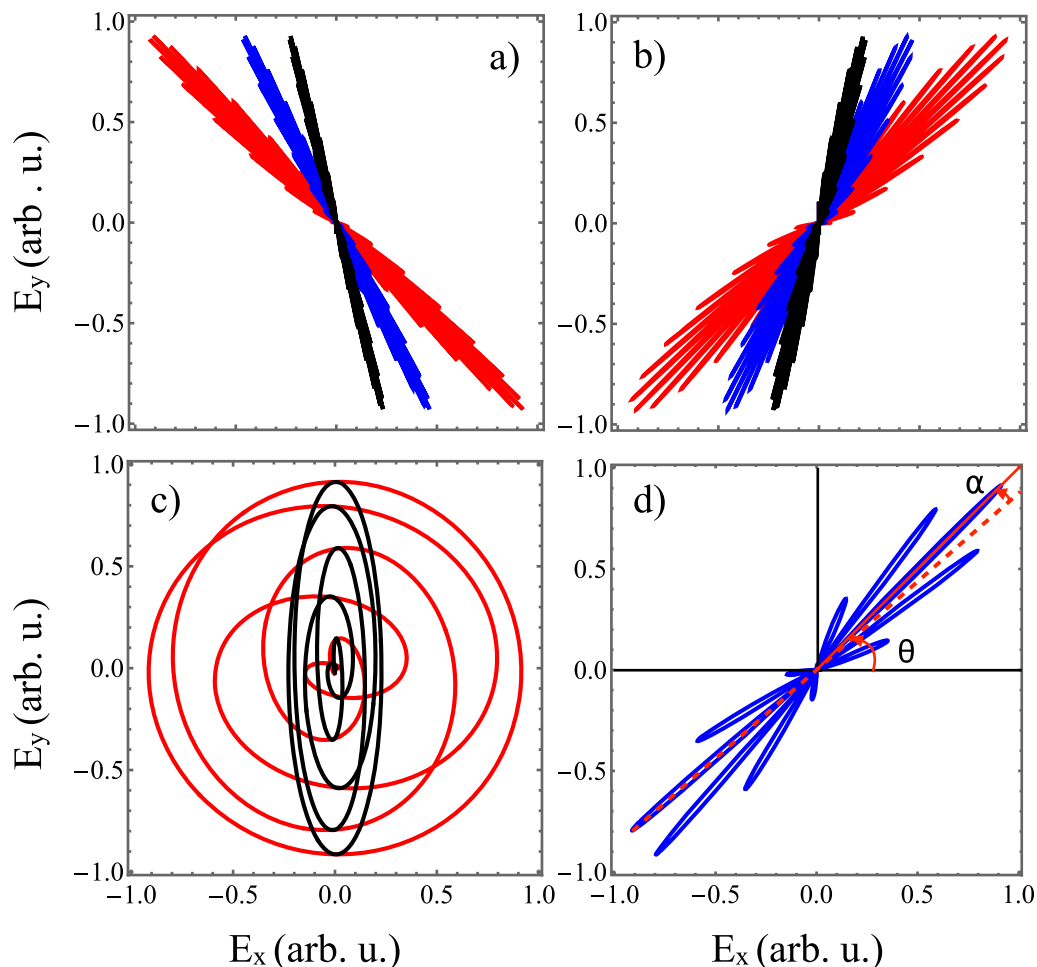


**Fig. 1** Polarization-crafted (PC) pulses. (a) Lissajous curves for  $\delta t = T/2$  and ratios  $\epsilon = 1, 1/2$  and  $1/4$  in red, blue and black, respectively. (b) Same as panel (a) but with  $\delta t = T$ . (c) Lissajous curves for  $\epsilon = 1$  (red solid curve) and  $1/4$  (black solid curve) with  $\delta t = T/4$ . In all cases, we set  $\phi = 0$  and  $n_c = 16$ . (d) Definition of the angles  $\theta$  and  $\alpha$  (see the text for more details)

the range  $\delta t = [0, T]$ . It is worth mentioning here that the simulation temporal window presented in this and the following sections will be adjusted accordingly to include both laser pulses completely. We also define the relative phase  $\phi = \phi_y - \phi_x$ . This quantity is instrumental for the control of the laser field shape, as we will see in the next sections. Notice that by forcing  $\phi_x = \phi_y$  and  $E_{0,x} = E_{0,y}$  one recovers the well-known AP pulses described, for instance, in Refs. [5, 20]. Here, however, we explore all the possible ways to fine-tune the polarization state of the driving laser field. In Ref. [5], the pulse temporal width, used to investigate HHG with Gaussian-shaped AP pulses, was set to  $2\Delta t$  and  $5\Delta t$  ( $\Delta t$  is the full width at half maximum), corresponding to  $\approx 6$  and  $15$  total optical cycles,  $n_c$ ,

### 2.1 Effect of the laser electric field amplitudes' ratio

By changing the ratio  $\epsilon = E_{0,y}/E_{0,x}$  between the laser field amplitude components in Eqs. (1a) and (1b), for a fixed time delay  $\delta t$ , it is possible to change the angle of

the total laser field with respect to the plane  $E_y = 0$ , i.e., we obtain a linear-like Lissajous curve. Furthermore, for certain values of  $\delta t$  (see next section), we get a circular-like Lissajous curve. Here, the change in the ratio shrinks the total laser field in the direction of the component with smaller amplitude. We show these general features in Fig. 1a and b.

We depict the Lissajous curves for 3 different laser field amplitudes' ratios  $\epsilon = 1, 1/2$  and  $1/4$  (red, blue and black curves in Fig. 1a and b, respectively), and two different time delays  $\delta t = T/2$  in Fig. 1a ( $T = 2\pi/\omega_0$  is the optical period) and  $\delta t = T$  in Fig. 1b, keeping the relative phase at the value  $\phi = 0$ . Figure 1c shows the resulting Lissajous figures for a time delay corresponding to  $\delta t = T/4$  and two different amplitudes' ratios,  $\epsilon = 1$  and  $1/4$ , in red and black, respectively. Experimentally, changing the ratio between the amplitudes of the laser field components corresponds to change the angle on the initial incident laser field with respect to the normal to the propagation direction. This change must be done before the laser field enters the birefrin-

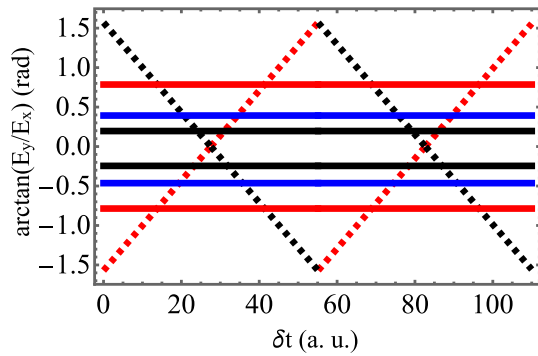


**Fig. 2** Temporal evolution of the angle,  $\theta$ , calculated from Eq. (2). The red, blue and black solid curves are the  $\theta$  values for the parameters used in Fig. 1a. In the same plot, the dashed red and dashed black curves are for the case of  $\varepsilon = 1$  and  $\delta t = T/4$  and  $\delta t = 3T/4$ , respectively

gent medium used to set their relative time delay [5, 26]. This initial incident angle corresponds, in our current description, to the angle  $\theta$ , measured it with respect to the plane defined for  $E_x = 0$ , as shown in Fig. 1d. For  $\varepsilon = 1$ ,  $\theta$  takes the values  $-\pi/4$  or  $\pi/4$ , for  $\delta t = T/2$  and  $T$ , respectively. For the same time delays and ratio  $\varepsilon = 1/2$  ( $\varepsilon = 1/4$ ),  $\theta$  takes the value  $\pm 0.35\pi$  ( $\pm 0.45\pi$ ). In the next section, we show how to analytically calculate the angle  $\theta$ .

### 2.2 Effect of the time delay

By changing the time delay  $\delta t$  in Eq. (1b), it is also possible to modify the shape of the Lissajous curves formed by the two orthogonal laser fields. For example, if the delay is set to  $\delta t = nT/2$ , with  $n$  an integer, the Lissajous curves have a distinct line-like shape. However, if  $\delta t = (2n - 1)T/4$  the Lissajous curves transform into a circular-like shape, defining a circular polarized laser field with time-dependent ellipticity. This time-dependent ellipticity steers the electron in such a way that the electron re-scattering with the parent ion is avoided. For a fixed laser electric field amplitudes' ratio,  $\varepsilon$ , it is possible to obtain the evolution of the angle,  $\theta$ , as a function of the time delay,  $\delta t$ . To calculate  $\theta$ , we use the expression  $\tan(\theta) = \varepsilon \sin(\omega(t - \delta t)) / \sin(\omega t)$ . Then,

$$\theta = \arctan \left( \varepsilon \frac{\sin(\omega(t - \delta t))}{\sin(\omega t)} \right) = \begin{cases} -\arctan(\varepsilon \cot(\omega t)), & \text{for } \delta t = T/4 \\ -\varepsilon\pi/4, & \text{for } \delta t = T/2 \\ \arctan(\varepsilon \cot(\omega t)), & \text{for } \delta t = 3T/4 \\ \varepsilon\pi/4, & \text{for } \delta t = T. \end{cases} \quad (2)$$

for a  $\sin^2$ -shaped pulse. This allows us to use a similar set of temporal parameters in the present contribution.

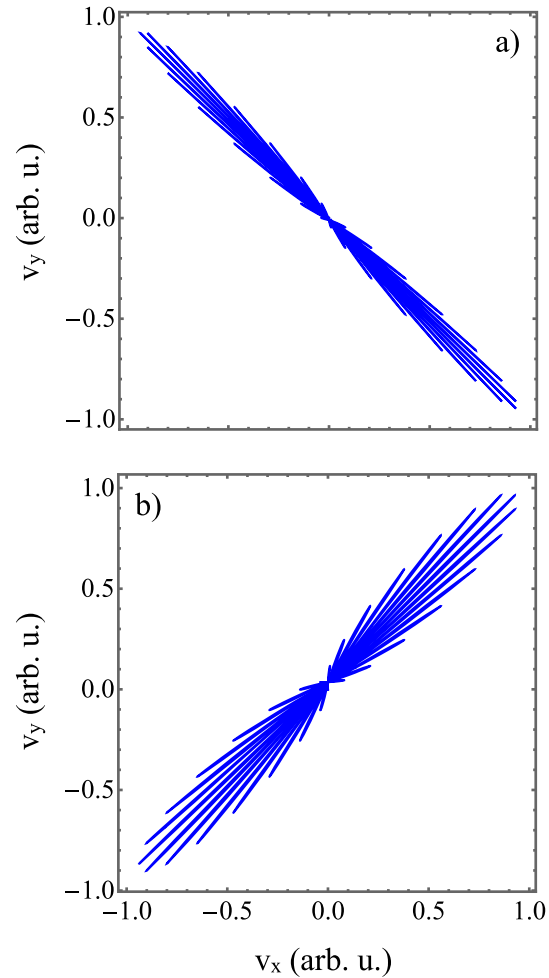


**Fig. 3** Classical electron velocity for (a)  $\delta t = T/2$  and (b)  $\delta t = T$ , calculated by integrating the two-dimensional classical equations of motion of an electron in the laser electric field given by Eqs. (1a) and (1b) (red curves in Fig. 1a and b). We use here  $E_0 = 0.0998$  (a. u.) and  $n_c = 15$  cycles

The different cases of Eq. (2) are presented in Fig. 2. Here, we depict in red, blue and black, the results of Eq. (2) with a time delay of  $\delta t = T/2$  and for  $\varepsilon = 1, 1/2$  and  $1/4$ , respectively. The dashed red and dashed black lines show the case for  $\varepsilon = 1$  and  $\delta t = T/4$  and  $\delta t = 3T/4$ , respectively. We can see that (i)  $\theta$  is constant during one full laser cycle for  $\delta t = nT/2$ , and (ii)  $\theta$  varies with time for  $\delta t = (n + 1)T/4$ .

From Eq. (2), we can define an AP laser field with constant polarization, e.g., setting  $\theta = \pi/4$ . Likewise, Eq. (2) includes AP laser fields with variable polarization as well, when  $\theta = \arctan(\cot(\omega t))$ . Notice that AP pulses are only possible if  $\phi_x = \phi_y = 0$  and  $\varepsilon = 1$ . From PC pulses, changes in time delays,  $\delta t$ , and amplitude ratios,  $\varepsilon$ , allow us to tailor the angle  $\theta$  and polarization state of the AP laser fields. Here, it is then interesting to ask: What is the final photoelectron momentum distribution when PC pulses interact with atoms?

To get insight about the electron dynamics, we can start calculating the resulting electron velocities

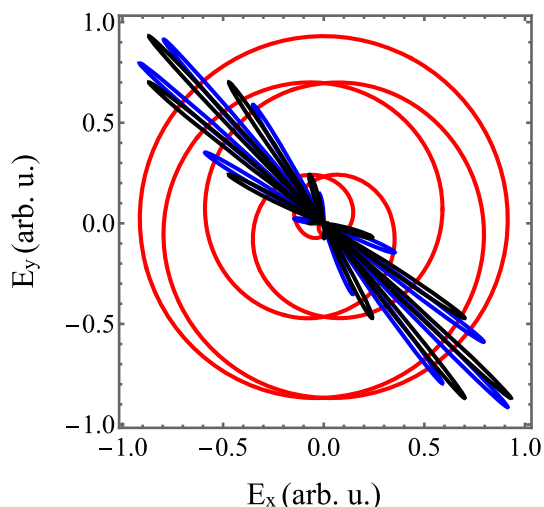


**Fig. 4** Parametric plots for different values of the laser field relative phase,  $\phi$ . In red and blue we plot the field’s parametric plot with  $\phi = \pi/2$  ( $\phi_x = 0, \phi_y = \pi/2$ ) and  $\phi = 0$  ( $\phi_x = 0, \phi_y = 0$ ). The time delay for both cases is the same,  $\delta t = 0$  and  $T/2$ , respectively. Notice that for the case of AP pulses, a relative phase change of  $\pi$  will only change the position of the petals and not the shape of the total laser field. This is shown by the black curve for which we used  $\phi = 0$  but with each laser field phase given by  $\phi_{x,y} = \pi/2$  and a time delay between the pulses of  $\delta t = T/2$

by solving the two-dimensional classical equations of motion for one free electron in the laser electric fields defined by Eqs. (1a) and (1b). Here, we set the time delays between the pulses as  $\delta t = T/2$  and  $\delta t = T$ . The results are presented in Fig. 3a and b, respectively. The classical electron velocities resemble the fields presented in Fig. 1a and b. It is important to mention that the classical velocities show a larger angular spreading as the delay between the pulses increases. This will have a clear impact on the ATI spectra, as we show in the next sections using the quantum mechanical simulations.

### 2.3 Angular distribution of the electron velocity

For linear-like PC fields and time delays values of  $T/2$  and  $T$ , it is possible to define the angle,  $\alpha$ , between the largest laser field amplitude oscillation and the following one, as shown in Fig. 1d. Since the angular velocity (momentum) distribution, Fig. 3, resembles the laser field shape, Fig. 1a and b, the angle  $\alpha$  is useful to investigate the angular distribution of the photoelectrons. To calculate such an angle, we compute the ratio between the laser electric field components envelopes. By expanding the ratio and taking only the linear terms in  $t$  and  $\delta t$ , we arrive to:

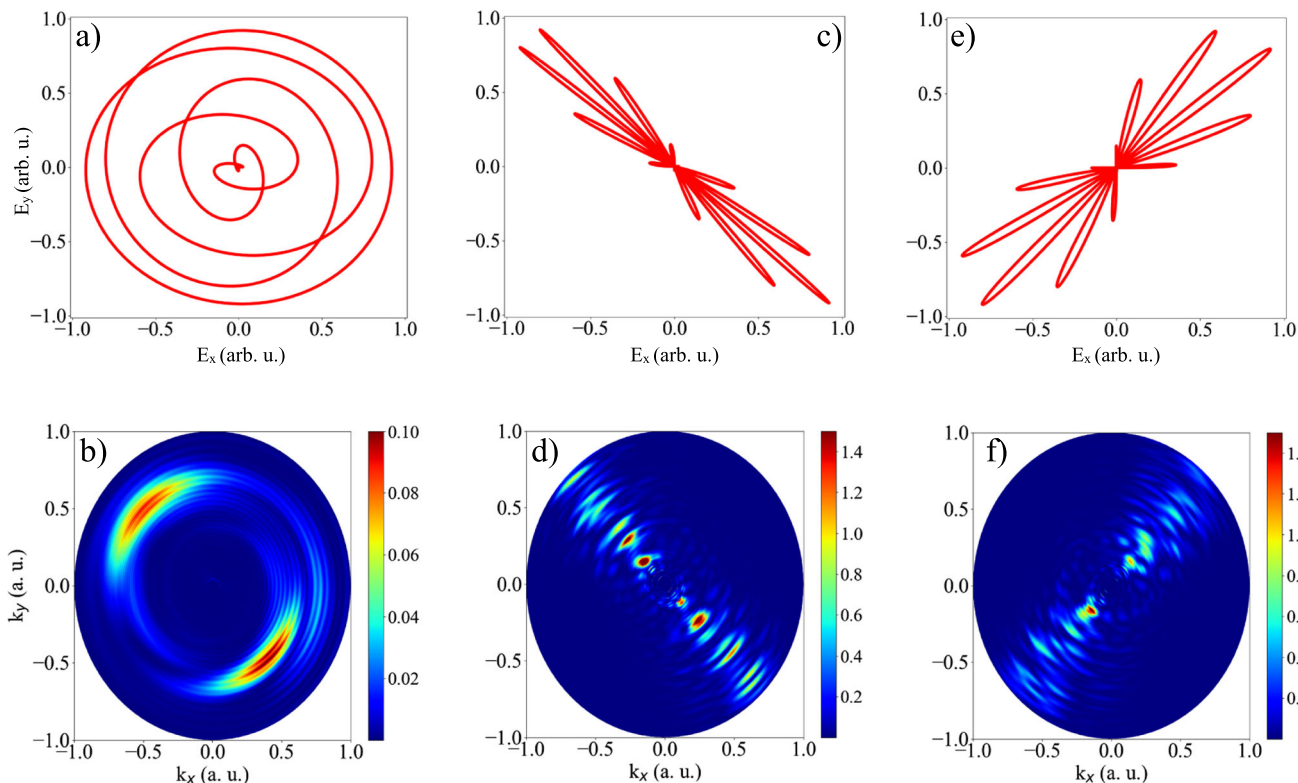


**Fig. 5** Parametric plots of the laser field components and generated 2D photoelectron momentum distribution for the case of short PC pulses. The relative time delay between the laser fields components is  $\delta t = T/4$  for (a) and (b),  $\delta t = T/2$  for (c) and (d) and  $\delta t = T$  for (e) and (f). It is clear from (d) and (f) that the angular aperture of the photoelectron momentum distributions increases with the time delay, as predicted by Eq. (3). For all the plots, we used  $\varepsilon = 1$  and  $n_c = 6$  cycles

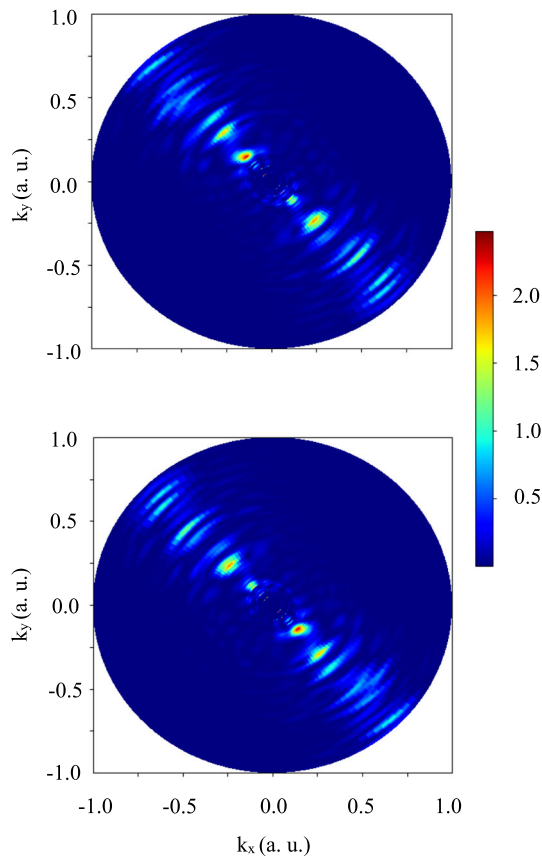


**Fig. 6** Effect of the relative phase in the 2D photoelectron momentum distributions. In (a), the relative phase between the laser fields is  $\phi = 0$  ( $\phi_x = \phi_y = 0$ ), in (b)  $\phi = \pi/2$  ( $\phi_x = \phi_y = \pi$ ). In all the cases,  $n_c = 6$  cycles

$$\alpha = \arctan \left( \frac{\varepsilon \sin^2(\omega(t - \delta t)/(2n_c))}{\sin^2(\omega t/(2n_c))} \right) - \varepsilon \frac{\pi}{4} \approx \arctan \left( \frac{2}{3} \varepsilon \frac{\omega^2 t}{n_c^2} \delta t \right) - \varepsilon \frac{\pi}{4} + O(\delta t^2). \tag{3}$$

The validity of Eq. (3) is restricted to small time delays around  $\delta t = T/2$  and  $\delta t = T$ , since for other time delay values, circular polarized fields appear, as shown in Fig 1c. For a laser field with  $n_c = 6$  cycles,  $\omega = 800$  nm,  $\delta t = T/2$  and  $t = T/2$ ,  $\alpha \approx 10^\circ$ . For the same laser parameters, but with  $n_c = 15$  cycles, Eq. (3) predicts a smaller angle,  $\alpha \approx 1^\circ$ . Thus, by increasing the number of cycles we can manipulate the collimation of the photoelectron momentum distribution when PC laser fields are used. Comparing Eq. (3) with the results presented in [5], we see a smaller increase in the angle as the time delay increases. However, Eq. (3) is more general, considering we have kept the ratio between the orthogonal laser field amplitudes. Overall, from Eq. (3), we can conclude that the angle between successive petals increases with the time delay. Con-

trarily, for a fixed time delay, by increasing the number of cycles, the photoelectron momentum distribution becomes more collimated around the angle,  $\theta$ . Likewise, we can use the ratio between the laser fields amplitudes to change the angular distribution of the electron momentum and the angle  $\alpha$ . This means that we can vary the amplitudes ratio to select the electron emission angle, as already shown in Fig. 1a. This is consistent with the fact that, reducing the amplitude of one of the laser fields components, the excursion of the electron in such a direction gets reduced as well. It is important to remark that the angular dependence of the photoelectron distributions with the number of cycles and the time delay is only valid for time delays that are multiple integers of  $T/2$ . For time delays that are multiple integers of  $T/4$ , the angle  $\theta$  has not meaning since it changes with time, as shown by Eq. (2).

### 2.4 Effect of the relative phase

Until now, we showed that the classical electron velocities can be tuned accordingly to the changes in the laser electric field components amplitudes ratio,  $\varepsilon$  and its relative time delay,  $\delta t$ . In addition, by modifying the CEPs  $\phi_x$  and  $\phi_y$  of each laser electric field components, we can change the Lissajous curves from a circular-like to a line-like shape. Thus, using the relative phase  $\phi$  we have three different methods to manipulate the electron dynamics. Figure 4 shows the parametric plots of the laser field components for a constant time delay  $\delta t = T/2$  and two different relative phases, namely  $\phi = 0$  (red solid line) and  $\phi = \pi/2$  (blue solid line). Here, the most remarkable feature is that the Lissajous curve is unique for a fixed pair of time delay,  $\delta t$ , and relative phase  $\phi$  (solid black line). Experimentally, this opens the possibility of characterizing the CEP: For example, by measuring the photoelectrons produced by ultrashort PC laser fields one could extract variations in the CEP from pulse to pulse if the time delay between the pulses is fixed. This is because the time delay,  $\delta t$ , together with the amplitude ratio of the laser field's components,  $\varepsilon$ , and the relative phase  $\phi$  define a unique Lissajous curve, which consequently gives rise to a unique photoelectron ATI spectra. This technique, however, would be limited to the degree of time delay stabilization. More importantly, the PC laser fields could provide a novel way to characterize the CEP for pulses with many cycles, where the direct CEP measurement is difficult.

### 3 ATI driven by short PC fields

In the previous sections, we demonstrated how the manipulation of the field's components amplitude ratio,  $\varepsilon$ , time delay,  $\delta t$ , and relative phase allows us to tailor the laser electric field, that, in turn, will produce distinct photoelectron distributions. Additionally, we illustrated that specific time delays can result in a laser pulse exhibiting time-dependent ellipticity. This occurs

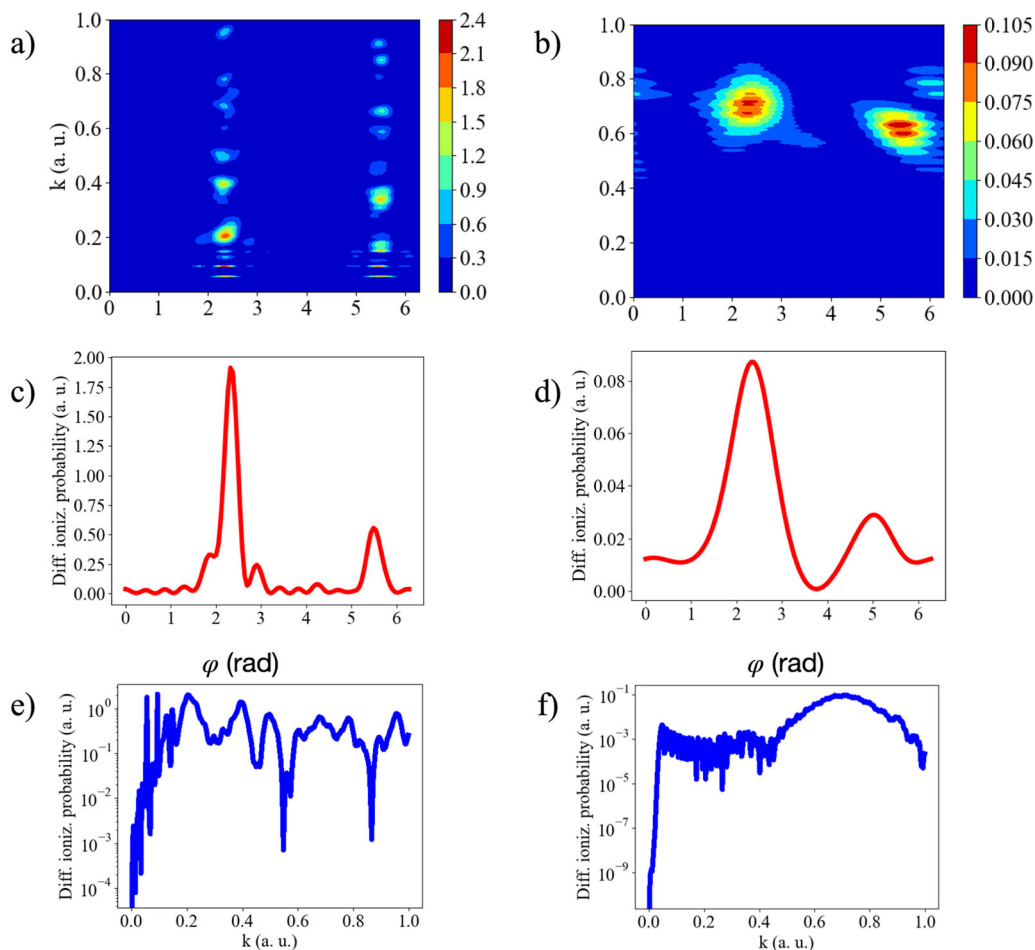


**Fig. 7** (a, b) 2D photoelectron momentum distributions plotted as Cartesian plots as a function of the polar angle,  $\varphi$ , and the photoelectron momentum,  $k$ ; (c) cut of the plot (a) at  $k = 0.2$  a.u.; (d) cut of the plot (b) at  $k = 0.7$  a.u.; (e, f) cut of the plots in (a) and (b) at  $\varphi = 2.3$ . In (a), (c) and (e)  $\delta t = T/2$  and in (b), (d) and (f)  $\delta t = T/4$

when  $\delta t = (2n - 1)T/4$ . Furthermore, the time delay between the laser electric field components determines whether the electron undergoes multiple re-scatterings with the parent ion or not. For example, a delay of  $\delta t = T/4$  leads to the total absence of re-scattering. Conversely, for  $\delta t = T/2$ , there are multiple re-scattering events as the electron intersects the ion position repeatedly. It is then instrumental to distinguish between these features to understand if the observed photoelectron spectra is formed by multiple re-scattering events and/or by intra-cycle interference [23]. This distinction is particularly important for molecular structure characterization [17].

In order to study how the different PC pulse configurations tailor the photoelectron spectra, we drive an hydrogen atom with short and long laser PC pulses and compute the 2D photoelectron momentum distributions, i.e., the distribution of final photoelectron momenta in an  $x - y$  plane, due to the action of the external laser field, using the 3D TDSE Q-prop solver [23]. For the case of short PC pulses, we set the number of cycles  $n_c = 6$  (total duration  $\approx 16$  fs) and the laser field central wavelength  $\lambda = 800$  nm ( $\omega = 0.057$

a.u.). Furthermore, the laser field amplitude is set to  $E_0 = 0.0534$  a.u., the amplitude ratio of the laser field’s components to  $\varepsilon = 1$ , and the CEP of each component as  $\phi_x = \phi_y = 0$ .

The calculated 2D photoelectron momentum distributions and laser electric field components are presented in Fig. 5. Figure 5a shows the parametric plots of the laser field components with a time delay  $\delta t = T/4$ . The resulting ATI spectrum is depicted in Fig. 5b. Here, the shape of the 2D photoelectron momentum distribution is typical for atoms driven by circularly polarized fields [27]. Figure 5c, e and d, f shows the corresponding parametric plot of the laser fields and the resulting 2D photoelectron momentum distribution for the case of a time delay  $\delta t = T/2$  ( $\delta t = T$ ). Several characteristics predicted by Eq. (3) for linear-like PC fields have a clear impact on the computed ATI 2D photoelectron momentum distributions, namely (1) the photoelectron momentum distributions closely follow the shape of the PC pulses, (2) Fig. 5c–f evidently shows that, for the specific time delays used, with an amplitudes ratio  $\varepsilon = 1$ , the angle is  $\theta = \pm\pi/4$ , and (3) the angular distribution angle,  $\alpha$ , increases with the time

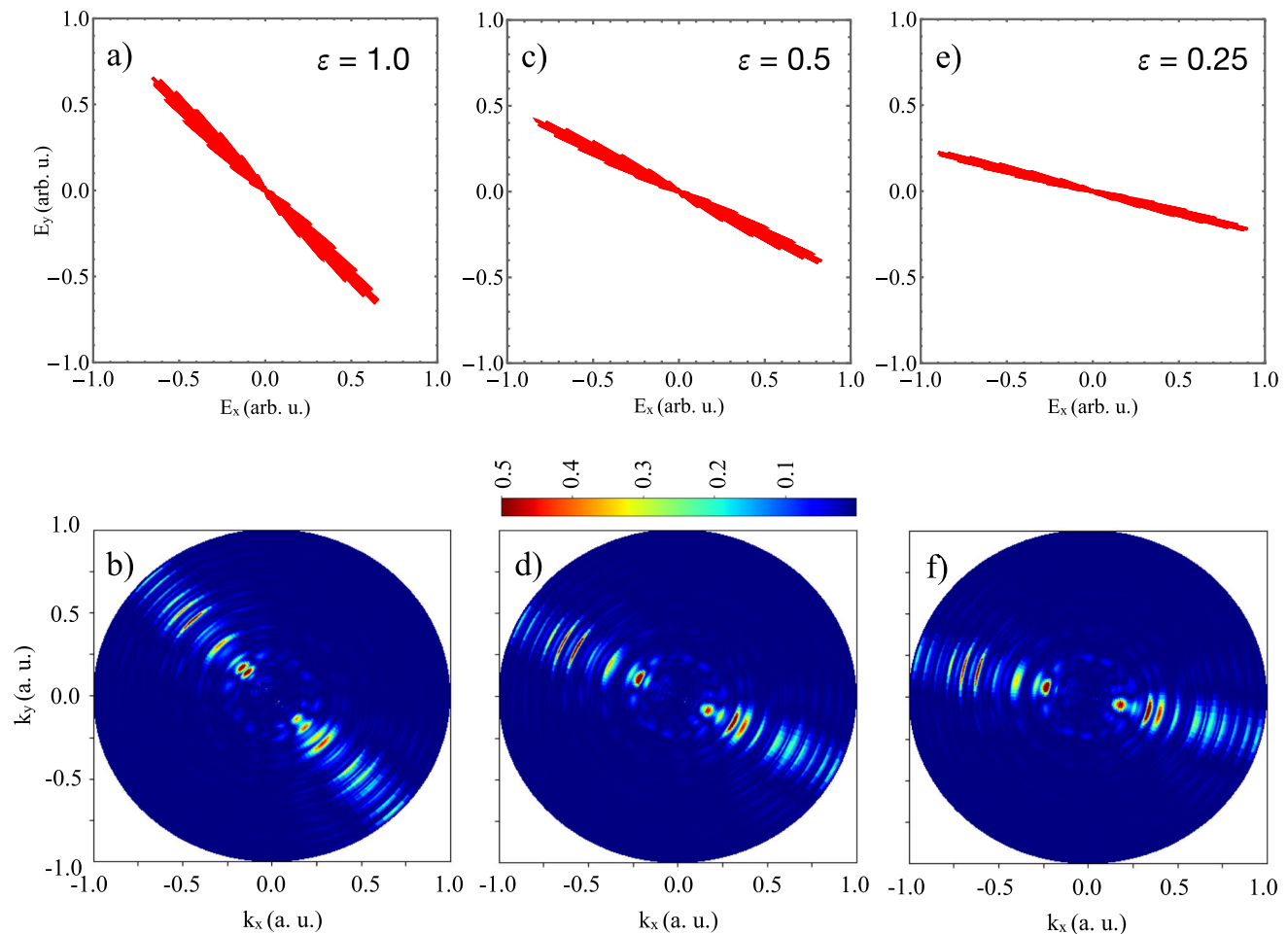


**Fig. 8** Parametric plots of the laser field components and generated 2D photoelectron momentum distribution for the case of long PC pulses. Here  $n_c = 16$  and the time delay  $\delta t = T/2$ . (a) and (b)  $\varepsilon = 1$ , (c) and (d)  $\varepsilon = 1/2$  and (e) and (f)  $\varepsilon = 1/4$

delay between the laser electric field components. This results in a more spread angular distribution in the 2D photoelectron momentum, as shown in Fig. 5d and f.

We investigate the effect of the CEP of the  $x$  and  $y$  laser field components in the 2D photoelectron momentum distribution. Figure 6 shows two different cases with the same relative phase  $\phi = 0$ , but different phases in the  $x$  and  $y$  field components, namely  $\phi_x = \phi_y = 0$  in Fig. 6a and  $\phi_x = \phi_y = \pi$  in Fig. 6b. We observe a flip of  $\pi$  in the structures for these two cases. The same features are observed between  $\phi_x = \phi_y = \pi/2$  and  $\phi_x = \phi_y = 3\pi/2$  (no shown here). It is worth mentioning, however, that it will not be possible, in principle, to fully characterize the CEP with this observable, given the fact that considerable changes in its value would be needed. (In our case, we have changed the individual phases by  $\pi$ .)

As shown previously, the 2D photoelectron momentum distributions generated with PC pulses (see Figs. 5 and 8 in the next section) closely follow the direction of the laser electric field. It is, however, important to dissect these 2D photoelectron momentum distributions,

in order to extract additional information, namely (a) the collimation of the photoelectron distributions and (b) the underlying physics.

To understand the differences in the 2D photoelectron distributions between particular cases of AP and PC pulses, in Fig. 7 we plot them now as a Cartesian plot, as a function of the polar angle,  $\varphi$ , and the photoelectron momentum,  $k$ . These spectra were computed using two different values for the time delay, namely Fig. 7a  $\delta t = T/2$  and Fig. 7b  $\delta t = T/4$ . The photoelectron distribution for  $\delta t = T/2$  shows narrow angular distributions around the angles  $3\pi/4$  and  $7\pi/4$ , distributed along the whole photoelectron momentum range (0-1 a.u.). This feature can be better observed if we make a “cut” at the photoelectron momentum values for which the photoelectron distributions exhibit a maximum. Thus, in Fig. 7c we use  $k = 0.2$  a.u. and in Fig. 7d  $k = 0.7$  a.u. From these plots, we can clearly notice that for  $\delta t = T/2$  the photoelectrons are emitted within a narrow angular range. Likewise, for  $\delta t = T/4$  the photoelectron distribution maxima are larger around the same angles, but they exhibit a collimation in the elec-



tron momentum as well (see the “islands” around to  $k \approx 0.6 - 0.8$  a. u.).

As discussed in Ref. [22], fields with variable polarization, like the one used to obtain Fig. 7, drive the electron away from the parent ion, preventing re-scattering (the laser-ionized electron misses the parent ion when the direction of the laser electric field reverses) and altering the emission times and trajectories. To analyze these aspects, we now focus on a particular polar angle,  $\phi = 2.3$  rad. In the energy region below  $2U_p$ , direct electron emission is dominant, so we focus our discussion on direct ATI. Distinct interference patterns are clearly observed in Fig. 7e and f. These features could be due to the interference of direct wave packets emitted at different ionization times. As demonstrated throughout the manuscript, the pulses used in our simulations significantly modify the electron dynamics (e.g., emission times and trajectories), making it likely that the observed interference pattern results from direct ATI. We plan to explore this feature further by implementing an SFA-based model, where direct and re-scattered contributions can be disentangled, in a follow-up publication.

## 4 ATI driven by long PC fields

We also investigate the 2D photoelectron momentum distributions for long PC pulses. Here, we use  $n_c = 16$  cycles ( $\approx 43$  fs) and  $\phi_x = \phi_y = 0$ . We show, in Fig. 8, the parametric plots for the laser field with different laser field amplitudes' ratios, namely (a)  $\varepsilon = 1$ , (c)  $\varepsilon = 1/2$  and (e)  $\varepsilon = 1/4$ . The resulting 2D photoelectron momentum distributions are presented in panels (b), (d) and (f), respectively. In all these cases, we have set  $\delta t = T/2$ . Once again, as predicted by Eq. (3), we can see that  $\theta$  is sensitive to the values of  $\varepsilon$ . As mentioned before, experimentally, this scenario corresponds to change the initial incidence angle of the fundamental field. Additionally, as predicted by Eq. (3) a slightly narrow angular dispersion is observed in the 2D photoelectron momentum distributions.

## 5 Conclusions

By solving the 3D time-dependent Schrödinger equation (TDSE), we have demonstrated that the photoelectron momentum distributions can be continuously tuned by using both short and long polarization-crafted (PC) laser fields. The uniqueness of these laser fields lies in their ability to finely adjust the laser field polarization through three distinct parameters: the amplitude ratio, the time delay and the relative phase between the orthogonal field components. These parameters play a crucial role in altering the angle of the electron momentum distribution and its angular spreading, ultimately affecting the collimation of the photoelectrons. Since these parameters effectively characterize the electron

momentum, additional information can be gleaned from the resulting ATI spectra. By fixing the time delay and the amplitude ratio, one could, in principle, independently characterize the carrier-envelope phase (CEP) of the pulse, although the sensitivity of the observables to this parameter appears to be relatively low. Moreover, although the experimental implementation of various PC laser fields may pose challenges, it is attainable within today's laser laboratories. Therefore, PC pulses offer additional means to customize photoelectron emission, enabling the generation of photoelectron distributions with desired angular and energy characteristics, for example.

**Acknowledgements** The present work is supported by the National Key Research and Development Program of China (Grant No. 2023YFA1407100) and Guangdong Province Science and Technology Major Project (Future functional materials under extreme conditions—2021B0301030005). M. F. C. and C. G. acknowledge financial support from the Guangdong Natural Science Foundation (General Program project No. 2023A1515010871). E. G. N. and L. R. acknowledges the Consejo Nacional de Investigaciones Científicas y Técnicas (CONICET).

## Declarations

**Data Availability Statement** This manuscript has no associated data or the data will not be deposited. [Authors' comment: Data sets generated during the current study are available from the corresponding author on reasonable request.]

## References

1. E. Ikonnikov, M. Paolino, J.C. Garcia-Alvarez, Y. Orozco-Gonzalez, C. Granados, A. Röder, J. Léonard, M. Olivucci, S. Haacke, O. Kornilov, S. Gozem, Photoelectron spectroscopy of oppositely charged molecular switches in the aqueous phase: theory and experiment. *J. Phys. Chem. Lett* **14**, 6061–6070 (2023)
2. J. Volaric, W. Szymanski, N.A. Simeth, B.L. Feringa, Molecular photoswitches in aqueous environments. *Chem. Soc. Rev.* **50**, 12377–12449 (2021)
3. F. Krausz, M. Ivanov, Attosecond physics. *Rev. Mod. Phys.* **81**, 163–234 (2009)
4. A.H. Zewail, Femtochemistry: atomic-scale dynamics of the chemical bond. *J. Phys. Chem. A* **104**, 5660–5694 (2000)
5. E. Neyra, F. Videla, D. Biasetti, M.F. Ciappina, L. Rebón, Twisting attosecond pulse trains by amplitude-polarization IR pulses. *Phys. Rev. A* **108**, 043102 (2023)
6. M. Isinger, R.J. Squibb, D. Busto, S. Zhong, A. Harth, D. Kroon, S. Nandi, C.L. Arnold, M. Miranda, J.M. Dahlström, E. Lindroth, R. Feifel, M. Gisselbrecht, A. L'Huillier, Photoionization in the time and frequency domain. *Science* **358**, 893–896 (2017)
7. P.M. Paul, E.S. Toma, P. Breger, G. Mullot, F. Augé, P. Balcou, H.G. Muller, P. Agostini, Observation of a

- train of attosecond pulses from high harmonic generation. *Science* **292**, 1689–1692 (2001)
8. M. Hentschel, R. Kienberger, C. Spielmann, G.A. Reider, N. Milosevic, T. Brabec, P. Corkum, U. Heinzmann, F. Krausz, Attosecond metrology. *Nature* **414**, 509–513 (2001)
  9. M. Lewenstein, K.C. Kulander, K.J. Schafer, P.H. Bucksbaum, Rings in above-threshold ionization: a quasiclassical analysis. *Phys. Rev. A* **51**, 1495–1507 (1995)
  10. N. Suárez, A. Chacón, M.F. Ciappina, J. Biegert, M. Lewenstein, Above-threshold ionization and photoelectron spectra in atomic systems driven by strong laser fields. *Phys. Rev. A* **92**, 063421 (2015)
  11. M. Lewenstein, P. Balcou, M.Y. Ivanov, A. L’Huillier, P.B. Corkum, Theory of high-harmonic generation by low-frequency laser fields. *Phys. Rev. A* **49**, 2117–2132 (1994)
  12. K.C. Kulander, Multiphoton ionization of hydrogen: a time-dependent theory. *Phys. Rev. A* **35**, 445–447 (1987)
  13. P. Hoerner, W. Li, H.B. Schlegel, Sequential double ionization of molecules by strong laser fields simulated with time-dependent configuration interaction. *J. Chem. Phys.* **155**, 114103 (2021)
  14. H.G. Muller, H.B. Heuvel, M.J. Wiel, Experiments on “Above-Threshold Ionization” of atomic hydrogen. *Phys. Rev. A* **34**, 236–243 (1986)
  15. D.B. Milošević, High-order above-threshold ionization by a few-cycle laser pulse in the presence of a terahertz pulse. *Phys. Rev. A* **105**, 053111 (2022)
  16. G.G. Paulus, F. Grasbon, H. Walther, P. Villorresi, M. Nisoli, S. Stagira, E. Priori, S.D. Silvestri, Absolute-phase phenomena in photoionization with few-cycle laser pulses. *Nature* **414**, 182–184 (2001)
  17. C.I. Blaga, J. Xu, A.D. DiChiara, E. Sistrunk, K. Zhang, P. Agostini, T.A. Miller, L.F. DiMauro, C.D. Lin, Imaging ultrafast molecular dynamics with laser-induced electron diffraction. *Nature* **483**, 194–197 (2012)
  18. M. Pullen, B. Wolter, A.-T. Le, M. Baudisch, M. Hemmer, A. Senftleben, C.D. Schröter, J. Ullrich, R. Moshhammer, C.D. Lin, J. Biegert, Imaging an aligned polyatomic molecule with laser-induced electron diffraction. *Nat. Commun.* **6**, 7262 (2015)
  19. M. Mirhosseini, O.S. Magaña-Loaiza, C. Chen, B. Rodenburg, M. Malik, R.W. Boyd, Rapid generation of light beams carrying orbital angular momentum. *Opt. Exp.* **21**, 30196–30203 (2013)
  20. A. Fleischer, E. Bordo, O. Kfir, P. Sidorenko, O. Cohen, Polarization-fan high-order harmonics. *J. Phys. B: At. Mol. Opt. Phys.* **50**, 034001 (2017)
  21. P. Koval, D. Bauer, Qprop: a schrödinger-solver for intense laser-atom interaction. *Comp. Phys. Commun.* **174**, 396–421 (2006)
  22. V. Mosert, D. Bauer, Photoelectron spectra with qprop and t-SURFF. *Comp. Phys. Commun.* **207**, 452–463 (2016)
  23. V. Tulskey, D. Bauer, Qprop with faster calculation of photoelectron spectra. *Comp. Phys. Commun.* **251**, 107098 (2020)
  24. K. Amini, J. Biegert, F. Calegari, A. Chacón, M.F. Ciappina, A. Dauphin, D.K. Efimov, C.F. Morisson Faria, K. Giergiel, P. Gnierek et al., Symphony on strong field approximation. *Rep. Prog. Phys.* **82**, 116001 (2019)
  25. W. Li, F. He, Generation and application of a polarization-skewed attosecond pulse train. *Phys. Rev. A* **104**, 063114 (2021)
  26. G. Karras, M. Ndong, E. Hertz, D. Sugny, F. Billard, B. Lavorel, O. Faucher, Polarization shaping for unidirectional rotational motion of molecules. *Phys. Rev. Lett.* **114**, 103001 (2015)
  27. D.B. Milošević, G.G. Paulus, D. Bauer, W. Becker, Above-threshold ionization by few-cycle pulses. *J. Phys. B: At. Mol. Opt. Phys.* **39**, 203–262 (2006)

Springer Nature or its licensor (e.g. a society or other partner) holds exclusive rights to this article under a publishing agreement with the author(s) or other rightsholder(s); author self-archiving of the accepted manuscript version of this article is solely governed by the terms of such publishing agreement and applicable law.